



## Photocatalytic activity of Ag-Ag<sub>3</sub>PO<sub>4</sub>/Cellulose aerogel composite for degradation of dye pollutants under visible light irradiation

Nguyen Thi Hoa, Nguyen Trung Tien, Le Hong Phong, Vu Van Tai, Pham Xuan Nui\*

*Department of Chemical Engineering, Hanoi University of Mining and Geology  
 18-Vien Street, Duc Thang Ward, Bac Tu Liem, Hanoi, Vietnam.*

*\*Email : phamxuannui@hmg.edu.vn*

### ARTICLE INFO

Received: 15/3/2021

Accepted: 25/6/2021

Published: 30/6/2021

#### Keywords:

Photocatalyst, Ag-Ag<sub>3</sub>PO<sub>4</sub>/Cellulose aerogel, photodegradation, dye pollutants

### ABSTRACT

In this research, Ag-Ag<sub>3</sub>PO<sub>4</sub>/Cellulose aerogel composite was synthesized using hydrothermal reduction and freeze-drying methods. By combining the photocatalytic activity of the semiconductor Ag-Ag<sub>3</sub>PO<sub>4</sub> and cellulose aerogel synthesized from agricultural waste sources, the synthesized Ag-Ag<sub>3</sub>PO<sub>4</sub>/Cellulose aerogel composite has overcome the disadvantages of pure Ag<sub>3</sub>PO<sub>4</sub> and significantly improved the photocatalytic activity. Structural characteristics, morphology, surface area of the materials were analyzed by X-ray diffraction (XRD), scanning electron microscopy (SEM), N<sub>2</sub> adsorption-desorption and UV-vis diffuse reflectance spectroscopy (UV-vis DRS) methods. From the obtained results, composite has narrow bandgap energy (2.275 eV) and excellent catalytic performance in the photodegradation of dye pollutants (99% MB and 77% RY 145 degraded after 4 h, and only a minor change in the efficiency observed after four consecutive tests). It demonstrates the development of new catalysts made from agricultural waste sources that show high stability, ease of fabrication and can operate in natural light for environmental remediation.

### Introduction

Industries are the primary sources of hazardous chemicals and wastewater such as drugs, dyes, pesticides, heavy metals and nitro compounds and their derivatives, thereby making water pollution a major problem for modern society [1]. According to a survey, about 10-15 % of the water environment is polluted by dyes during the production process. Some of them even have high stability and degrading difficulty, thus endanger human health, plants and animals [2]. Over the past few decades, research on semiconductor photocatalytic materials has grown tremendously due to their potential to solve energy

shortage and environmental degradation [3,4]. Scientists hope to develop semiconductor materials that operatable under a wide range of light, high electron separation ability and sufficient charge to degrade dyes and harmful substances [5].

Photocatalytic degradation under visible light attracts attention intending to degrade organic dyes wastes from chemical, textile, dyeing factories. Compared with the photochemical method using ultraviolet radiation, this method has advantages such as simple synthesis route, low cost and high efficiency [6-8]. In 2010, Ye *et al.* [9] first researched and proved the photo-oxidation properties of Ag<sub>3</sub>PO<sub>4</sub> with bandgap energy E<sub>g</sub> of 2.36 eV. Then, this material was widely studied in water

oxidation and degradation of organic compounds under irradiation. When the irradiated light wavelength is above 420 nm,  $\text{Ag}_3\text{PO}_4$  has outstanding quantum separation and photocatalytic activity [10]. Many studies also reported that the surface plasmon resonance effect of  $\text{Ag}^0$  could enhance the activity and stability of  $\text{Ag}_3\text{PO}_4$  [11-13]. However, the nano-sized  $\text{Ag}/\text{Ag}_3\text{PO}_4$  is easily agglomerated in an aqueous solution, thus significantly reducing photocatalytic activity. In practical applications,  $\text{Ag}/\text{Ag}_3\text{PO}_4$  is also difficult to recover from the environment with simple methods and could lead to secondary pollution. The fixation of nano photocatalysts on supporting materials is considered one of the easiest and effective ways to overcome these limitations. Up to now, various materials have been developed as carriers, such as carbon materials [14,15], metal oxides [16,17] and organic compounds [18,19].

Currently, the most commonly used aerogel for photocatalytic applications is graphene aerogel. F. Chen *et al.* [20] synthesized graphene aerogel with 3D structure to support the  $\text{Ag}@\text{Ag}_3\text{PO}_4$  photocatalytic catalyst used for treating dyes in water. The results showed that the 3D  $\text{Ag}@\text{Ag}_3\text{PO}_4/\text{graphene}$  aerogel has good photoadsorption and photodegradation with both anionic and cationic dyes. S. Dong *et al.* [21] synthesized 3D  $\text{Bi}_2\text{WO}_6/\text{graphene}$  aerogel composite with excellent photocatalytic performance. Using graphene aerogel with its 3D structure, the material has narrower bandgap energy, improved light absorbability, higher charge separation efficiency and better-contaminated adsorption than the original  $\text{Bi}_2\text{WO}_6$ .

Cellulose aerogel is a form of gas-solid material produced from agricultural by-products (bagasse, straw, coffee beans,...). Since cellulose aerogel has most of the volume filled with air and gases, it resulted in a solid with extremely low density. However, the material still can withstand a weight of 500–2000 times its own [22]. Cellulose aerogel possesses excellent properties, suitable for applications in various fields: low density, high porosity, large specific surface area, good sound insulation, low heat transferability, good pollutant adsorbability, thermal and chemical stability, and biodegradability [23,24].

In this work, the  $\text{Ag}-\text{Ag}_3\text{PO}_4/\text{Cellulose}$  aerogel photocatalysts were synthesized using cellulose aerogel as a carrier to reduce the recombination of the photogenerated electron-hole pairs. We proposed bagasse, a cheap and abundantly available material in Vietnam, to synthesis cellulose. The degradation of

Methylene Blue (MB) and Reactive Yellow 145 (RY 145) dyes was used to investigate the photocatalytic activity of  $\text{Ag}-\text{Ag}_3\text{PO}_4/\text{Cellulose}$  aerogel composite.

## Experimental

### Materials

Polyvinyl alcohol (PVA), ethanol ( $\text{C}_2\text{H}_5\text{OH}$  99 %), sodium hydroxide ( $\text{NaOH}$  99 %), hydrogen peroxide ( $\text{H}_2\text{O}_2$  30 %), chloride acid ( $\text{HCl}$  38 %), sodium hypochlorite ( $\text{NaClO}$  99 %), silver nitrate ( $\text{AgNO}_3$ ) and sodium phosphate ( $\text{NaH}_2\text{PO}_4 \cdot \text{H}_2\text{O}$ ) were purchased from Sinopharm Chemical Reagent Co. Ltd., China. Methylene Blue (MB) and Reactive Yellow 145 (RY 145) were purchased from Merck, Germany. Sugarcane bagasse was used as the precursor of cellulose, collected from plantations located in Hoa Binh Province, Vietnam.

### Synthesis of $\text{Ag}-\text{Ag}_3\text{PO}_4/\text{Cellulose}$ aerogel composite

#### Extraction of cellulose from sugarcane bagasse

The bagasse was washed thoroughly and cut into 1-2 cm pieces, then grind into powder. The powder of sugarcane bagasse was dewaxed using ethanol/water (1:1 v/v), stirred for 2 h at 60 °C, then washed with deionized water. After removing impurities, the sugarcane bagasse was further treated with 1M  $\text{NaOH}$  solution at 80 °C in 2 h to remove lignin. The product was washed with deionized water until the neutral pH was reached. Subsequently, the product was treated using 1%  $\text{NaOH}$  and 1%  $\text{NaClO}$  (w/v) water solution with a molar ratio of 2:1 at 80 °C for 1.5 h to remove hemicellulose. The product mixture was filtered, washed with deionized water and dried at 60 °C overnight. Finally, the extracted cellulose had the form of a white powder.

#### Synthesis of $\text{Ag}-\text{Ag}_3\text{PO}_4/\text{Cellulose}$ aerogel composite

A mixture of cellulose and PVA with a molar ratio of 100:1 was dispersed 50 mL of deionized water. Then, this mixture was ultrasonicated for 10 min. The sample was put into a mold with dimensions of 10 cm x 10 cm x 3 cm and freeze for 24 h. After freezing, the sample is taken out and left at room temperature within 2 hours then freeze again within 12 hours.

The reduction–hydrothermal reaction of  $\text{AgNO}_3$  with hydrogel cellulose was proceeded by dispersing

cellulose gel in AgNO<sub>3</sub> solution with the concentrations of 0.05, 0.1 and 0.4 mol/L. The mixture was put in an autoclave for aging at 80 °C for 24 h. Hydrogel cellulose was washed with deionized water and dispersed into a 200 mL mixture of Na<sub>2</sub>HPO<sub>4</sub> 0.2 M and H<sub>2</sub>O<sub>2</sub> 30 % for 30 mins at room temperature. The mixture of hydrogel cellulose containing Ag-Ag<sub>3</sub>PO<sub>4</sub> was washed three times with deionized water and then put into molds with dimensions of 10 cm x 10 cm x 3 cm, then frozen at -5 °C for 24 h. Next, the sample was freeze-drying at -55 °C and vacuum pressure approximately at 10 μPa. Ag-Ag<sub>3</sub>PO<sub>4</sub>/Cellulose aerogel

composites are denoted as 0.05Ag-Ag<sub>3</sub>PO<sub>4</sub>/Cellulose aerogel, 0.1Ag-Ag<sub>3</sub>PO<sub>4</sub>/Cellulose aerogel và 0.4Ag-Ag<sub>3</sub>PO<sub>4</sub>/Cellulose aerogel, respectively with the concentrations of AgNO<sub>3</sub> solution. Figure 1 shows (a) composite gel, (b-d) 0.05Ag-Ag<sub>3</sub>PO<sub>4</sub>/Cellulose aerogel, 0.1Ag-Ag<sub>3</sub>PO<sub>4</sub>/Cellulose aerogel and 0.4Ag-Ag<sub>3</sub>PO<sub>4</sub>/Cellulose aerogel, (e) cross-linking between cellulose from bagasse and PVA chain, hydrogen bonds were formed between different hydroxyl functional groups of cellulose and PVA [25], (f-g) mechanism of hydrothermal reduction to form Ag<sup>0</sup> and Ag<sub>3</sub>PO<sub>4</sub>.

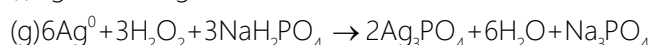
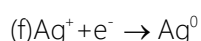
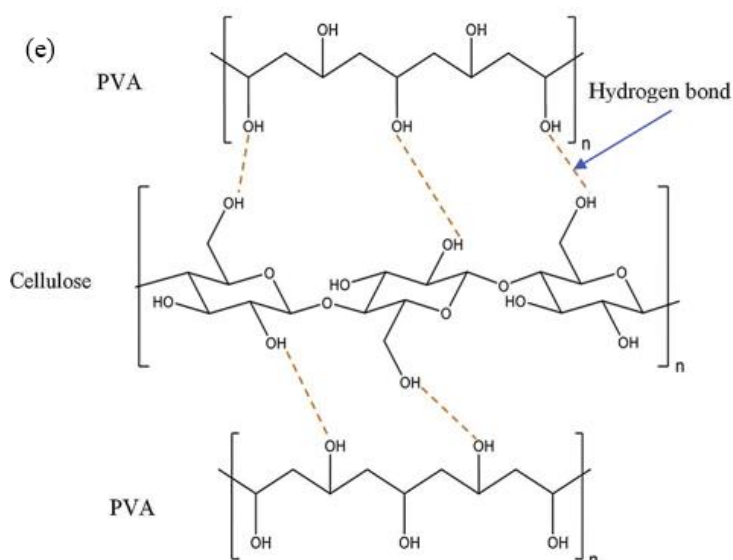
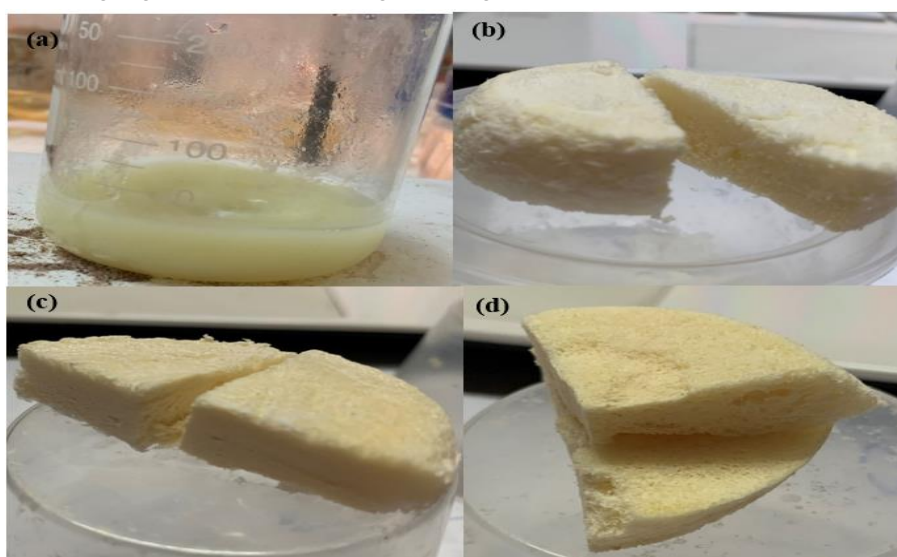


Figure 1: (a) the composite gel, (b-d) 0.05Ag-Ag<sub>3</sub>PO<sub>4</sub>/Cellulose aerogel, 0.1Ag-Ag<sub>3</sub>PO<sub>4</sub>/Cellulose aerogel và 0.4Ag-Ag<sub>3</sub>PO<sub>4</sub>/Cellulose aerogel, (e) cross-linking between cellulose from bagasse and PVA chain, (f-g) mechanism of hydrothermal reduction to form Ag<sup>0</sup> and Ag<sub>3</sub>PO<sub>4</sub>

## Characterization

X-ray diffraction spectrum (XRD) of the samples was measured on the Bruker D8 Advance diffractometer using Cu X-ray emission tube with wavelength  $\lambda(\text{CuK}\alpha) = 0.15406$  nm, capacity 30 kV, current 0.01 A were recorded in the  $2\theta$  range of 5–80°. All samples were ground into powder to avoid the influence of the crystalline orientation. The crystalline size ( $D$ ) of the sample for the (210) plane of  $\text{Ag}_3\text{PO}_4$  nanoparticle was calculated by the Scherrer formula [26]:

$$D = \frac{0.9\lambda}{\beta \times \cos\theta} \quad (1)$$

Where  $\lambda = 0.15406$  nm,  $\beta$  is the corrected integral width, and  $\theta$  is the Bragg angle. Surface morphology was observed by scanning electron microscopy method (S-4800, Hitachi). Specific surface area Brunauer–Emmett–Teller (BET) was determined at 77 K by the  $\text{N}_2$  adsorption-desorption method on ChemBET-3030. Ultraviolet-visible diffuse reflectance spectroscopy (Uv-Vis DRS) was recorded on UV-2600 (Shimadzu) spectrophotometer.

The point of zero charge ( $pzc$ ) of  $\text{Ag-Ag}_3\text{PO}_4/\text{Cellulose}$  aerogel was measured by salt addition method [27]. Typically, 50 mg of each sample was dispersed in 50 mL of KCl 0.1 M in 100 mL flasks and stirred magnetically for 30 min. The initial pH values ( $\text{pH}_0$ ) of the suspension were then adjusted between 2 and 12 by adding either HCl 0.25 M or NaOH solution, measured by a calibrated Hach pH201 pH meter with accuracy =  $\pm 0.02$ . After stirring for 24 h in a revolving water bath to reach equilibrium, resulting pH values were measured and the difference

between the initial and final pH values ( $\Delta\text{pH} = \text{pH} - \text{pH}_0$ ) against the initial pH was plotted. The pH value where  $\Delta\text{pH}$  equals zero was denoted  $\text{pH}_{pzc}$ .

## Catalytic activity test

The catalytic activity was evaluated through the degradation reaction of MB and RY 145 dyes under solar irradiation. Specifically, 50 mg of the photocatalyst was dispersed in 35 mL of an aqueous solution containing dyes (50 ppm). Before the reaction, the mixture was stirred magnetically at 300 rpm in the dark for 60 mins to achieve the adsorption-desorption equilibrium. The initial concentration ( $C_0$ ) was taken at this point. Then, the mixture was illuminated under natural light for 4 h (from 10 A.M. to 2 P.M.). After every hour, a small quantity of the solution was taken and measured under UV-Vis spectrometer to record the concentration ( $C_t$ ) (the absorption peaks of MB and RY 145 are at 664 nm and 541 nm, respectively). The dye degradation efficiency was calculated using Equation 2

$$\text{H\%} = \frac{C_0 - C_t}{C_0} \times 100 \quad (2)$$

Where:  $C_0$  is the initial dye concentration (ppm)

$C_t$  is the concentration of dye at time  $t$  (ppm)

## Results and Discussion

The crystal structure and phase composition of the samples were characterized by X-ray diffraction. The results are shown in Figure 2.

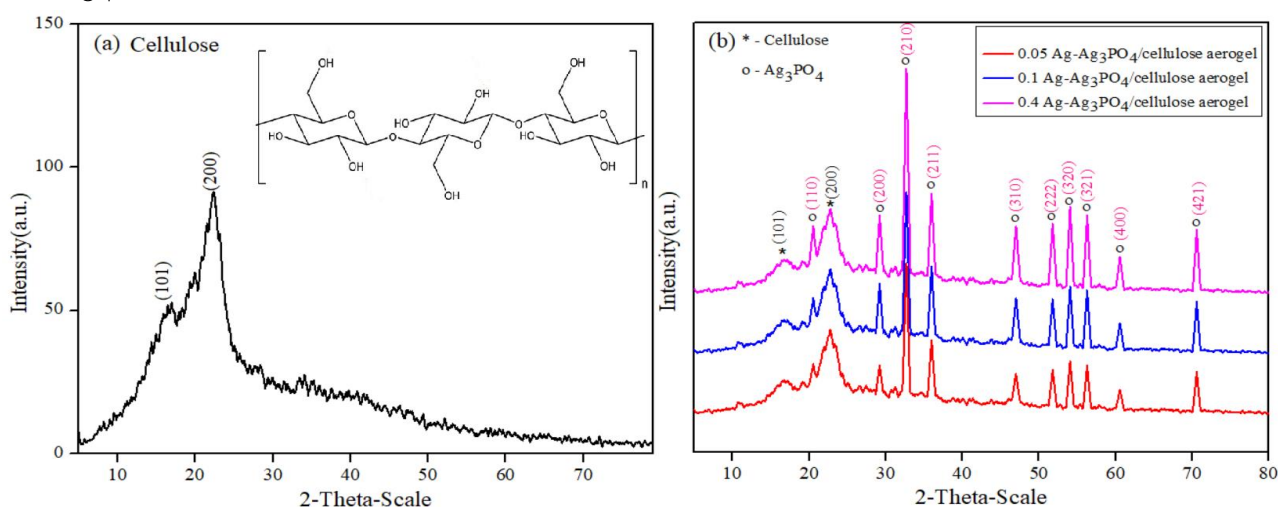


Figure 2: X-ray diffraction patterns of (a) cellulose, (b) 0.05 $\text{Ag-Ag}_3\text{PO}_4/\text{Cellulose}$  aerogel, 0.1 $\text{Ag-Ag}_3\text{PO}_4/\text{Cellulose}$  aerogel, 0.4 $\text{Ag-Ag}_3\text{PO}_4/\text{cellulose}$  aerogel

The characteristic diffraction peaks of cellulose aerogel were detected at  $2\theta = 16-17^\circ$ , corresponded to the (101) plane,  $19-20^\circ$  angle for amorphous phase and  $22^\circ$  angle for reflectant (200) [28]. Typical diffraction peaks of  $\text{Ag}_3\text{PO}_4$  were observed at  $2\theta = 20.88^\circ, 29.70^\circ, 33.29^\circ, 36.59^\circ, 47.79^\circ, 52.70^\circ, 55.02^\circ, 57.28^\circ, 61.64^\circ$  and  $71.90^\circ$ , corresponded to (110), (200), (210), (211), (310), (222), (320), (321), (400) and (421) crystal planes, respectively. The diffraction peaks can be indexed to the pure body-centered cubic (bcc) structure of  $\text{Ag}_3\text{PO}_4$ . The results were consistent with the standard data (JCPDS No. 06-0505). However, there were no visible diffraction peaks of Ag, which could be explained by either its small quantity or the small size of the particles. This phenomenon has been reported in previous papers of Ag/AgX (X: Cl, Br, I) [29,30]. All

diffraction patterns of 0.05Ag- $\text{Ag}_3\text{PO}_4$ /Cellulose aerogel, 0.1Ag- $\text{Ag}_3\text{PO}_4$ /Cellulose aerogel and 0.4Ag- $\text{Ag}_3\text{PO}_4$ /Cellulose aerogel samples appeared characteristic diffraction peaks of cellulose and  $\text{Ag}_3\text{PO}_4$ . Additionally, peak intensities increased when the concentration of  $\text{AgNO}_3$  increased from 0.05 to 0.4 M. This can be explained as the concentration of  $\text{AgNO}_3$  increases, more nanoparticles form and agglomerate. Using Scherrer equation, the size of  $\text{Ag}_3\text{PO}_4$  particles were estimated corresponding to (210) plane, approximately 17 nm for 0.05 Ag- $\text{Ag}_3\text{PO}_4$ /Cellulose aerogel sample and increased to 22 nm for 0.4 Ag- $\text{Ag}_3\text{PO}_4$ /Cellulose aerogel sample.

Scanning electron microscopy (SEM) was used to determine the surface morphology of 0.1Ag- $\text{Ag}_3\text{PO}_4$ /Cellulose aerogel composite (Figure 3).

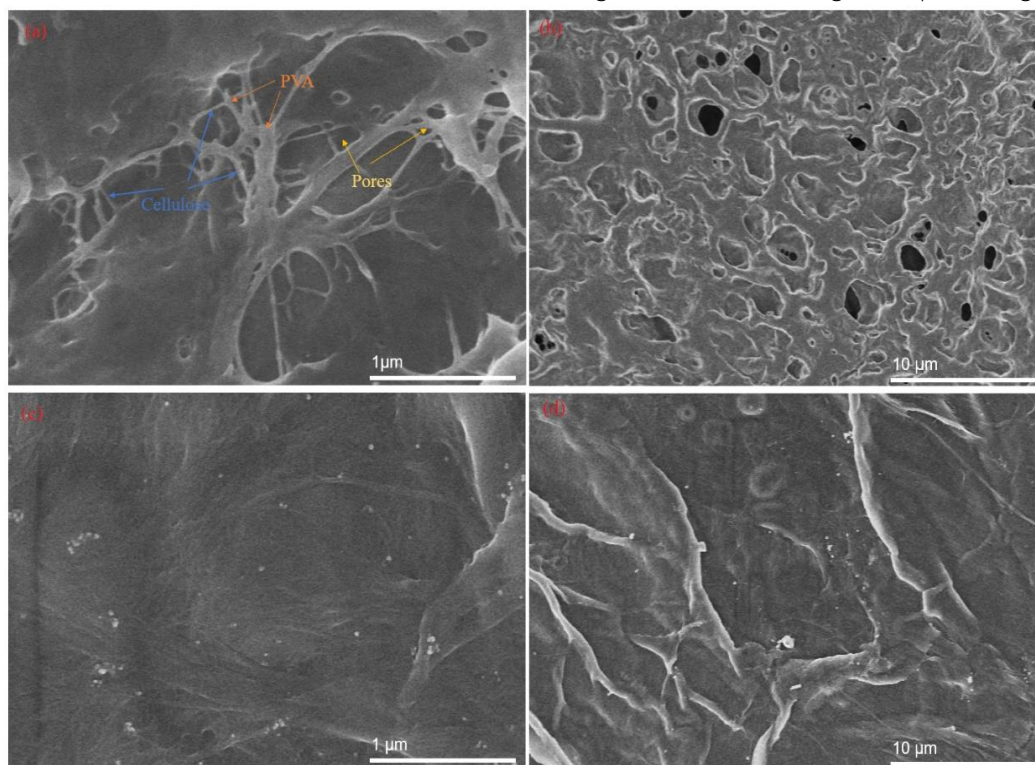


Figure 3: SEM images of (a-b) cellulose aerogel and (c-d) 0.1Ag- $\text{Ag}_3\text{PO}_4$ /cellulose aerogel

From the SEM images, after the freeze-drying process and solution evaporation, pores were formed with the size from nanometers to micrometers. Cellulose aerogel materials formed by random bonds between cellulose and PVA molecules created a 3-D network with high porosity.

Figure 3 (c,d) show that silver and  $\text{Ag}_3\text{PO}_4$  nanoparticles were synthesized in situ in cellulose aerogel and bonded directly to its frame by

electrostatic interaction with the hydroxyl groups of cellulose [31,32]. The porous structure of cellulose aerogel served both as cavities for the formation of the Ag- $\text{Ag}_3\text{PO}_4$  nanoparticles and shells to protect the nanostructure.

The surface area and pore size of cellulose aerogel and 0.1Ag- $\text{Ag}_3\text{PO}_4$ /Cellulose aerogel composite were determined by the  $\text{N}_2$  adsorption-desorption method (Figure 4).

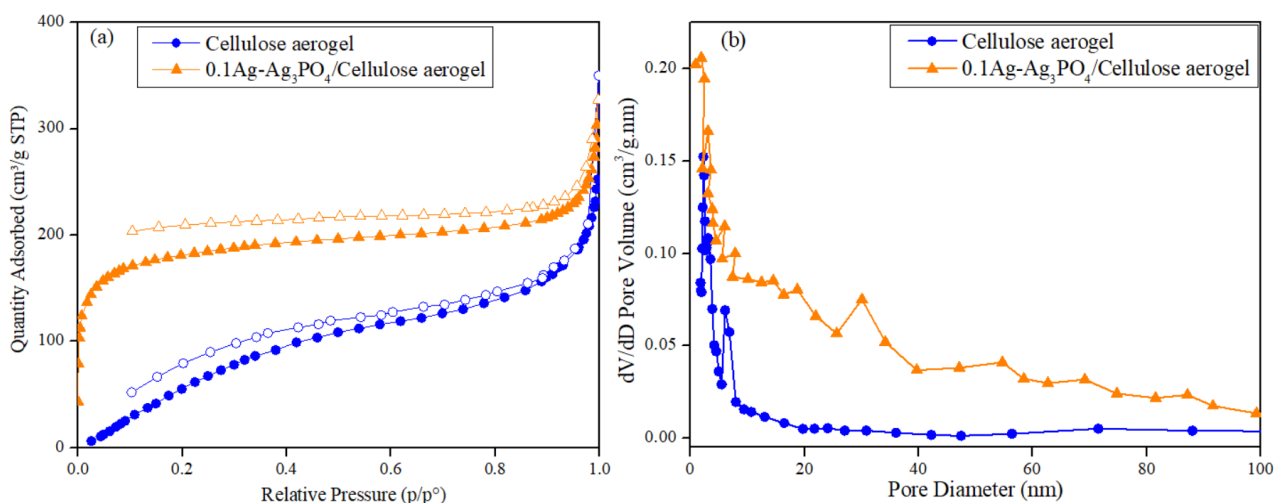


Figure 4: (a) N<sub>2</sub> adsorption-desorption isotherm curve (b) the corresponding pore size distribution of cellulose aerogel and 0.1Ag-Ag<sub>3</sub>PO<sub>4</sub>/Cellulose aerogel

The N<sub>2</sub> adsorption-desorption isotherm curve of cellulose aerogel and 0.1Ag-Ag<sub>3</sub>PO<sub>4</sub>/Cellulose aerogel composite (Figure 4a) have the type I hysteresis curve characteristic for capillary condensation and many defects in the sample. Based on Barrett-Joyner-Halenda (BJH) equation, the pore diameter of cellulose aerogel and 0.1Ag-Ag<sub>3</sub>PO<sub>4</sub>/Cellulose aerogel distributed widely in the range of 2–100 nm (**Error! Reference source not found.**b). BET specific surface area of 0.1Ag-Ag<sub>3</sub>PO<sub>4</sub>/Cellulose aerogel composite materials increased compared to cellulose aerogel.

Specifically, the surface area increased from 70 m<sup>2</sup>/g to 87.2 m<sup>2</sup>/g due to the formation of Ag<sub>3</sub>PO<sub>4</sub> and their uniform pore distribution. The adsorption surface area increased with the cross-section area with the pollutants, thereby increasing the photocatalytic efficiency of the composite.

Optical properties have a significant impact on the photocatalytic activity of the catalyst. Therefore, the absorption property of samples was investigated by the UV-vis diffuse reflectance spectroscopy and the results are shown in Figure 5.

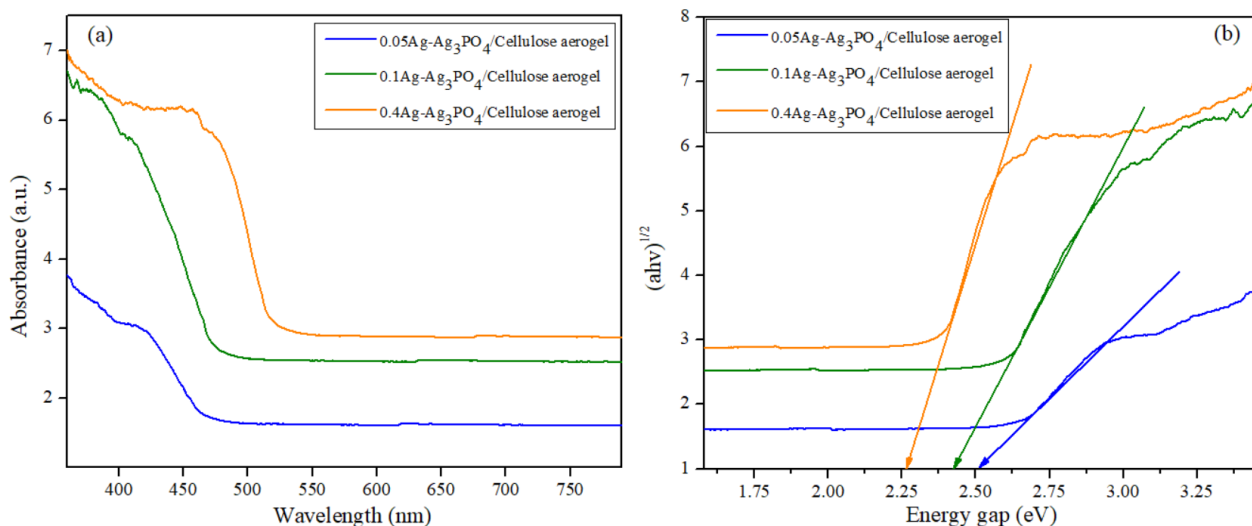


Figure 5: (a) UV-vis diffuse reflectance spectrum, (b) Kubelka-Munk equation of 0.05Ag-Ag<sub>3</sub>PO<sub>4</sub>/Cellulose aerogel, 0.1Ag-Ag<sub>3</sub>PO<sub>4</sub>/Cellulose aerogel and 0.4Ag-Ag<sub>3</sub>PO<sub>4</sub>/Cellulose aerogel

The absorption edge of the samples shifted to a greater wavelength region, from 495 to 540 nm as the concentration of AgNO<sub>3</sub> increased from 0.05 M to 0.4 M. The bandgap energies of the samples were also estimated using the Kubelka-Munk equation [33] :

$$\alpha h\nu = k(h\nu - E_g)^{\frac{n}{2}} \quad (3)$$

In which  $\alpha$ ,  $\nu$ ,  $k$  are the absorption coefficient, frequency of light and correction factor, respectively. The bandgap energy of 0.05Ag-Ag<sub>3</sub>PO<sub>4</sub>/Cellulose

aerogel, 0.1Ag-Ag<sub>3</sub>PO<sub>4</sub>/Cellulose aerogel, 0.4Ag-Ag<sub>3</sub>PO<sub>4</sub>/Cellulose aerogel samples were 2.51, 2.385 and 2.275 eV, respectively. The reduced bandgap energy was related to the surface plasmon absorption of silver metal on Ag<sub>3</sub>PO<sub>4</sub> surface [11]. Thus, increasing the content of active phase in composite materials has contributed to the bandgap energy reduction, while

increasing its photocatalytic efficiency. This result was entirely consistent with the previous report of Y. Liu *et al.* [12].

The photocatalytic activity of the samples was estimated by the degradation reaction of MB and RY 145 under visible light. The results are shown in Figure 6.

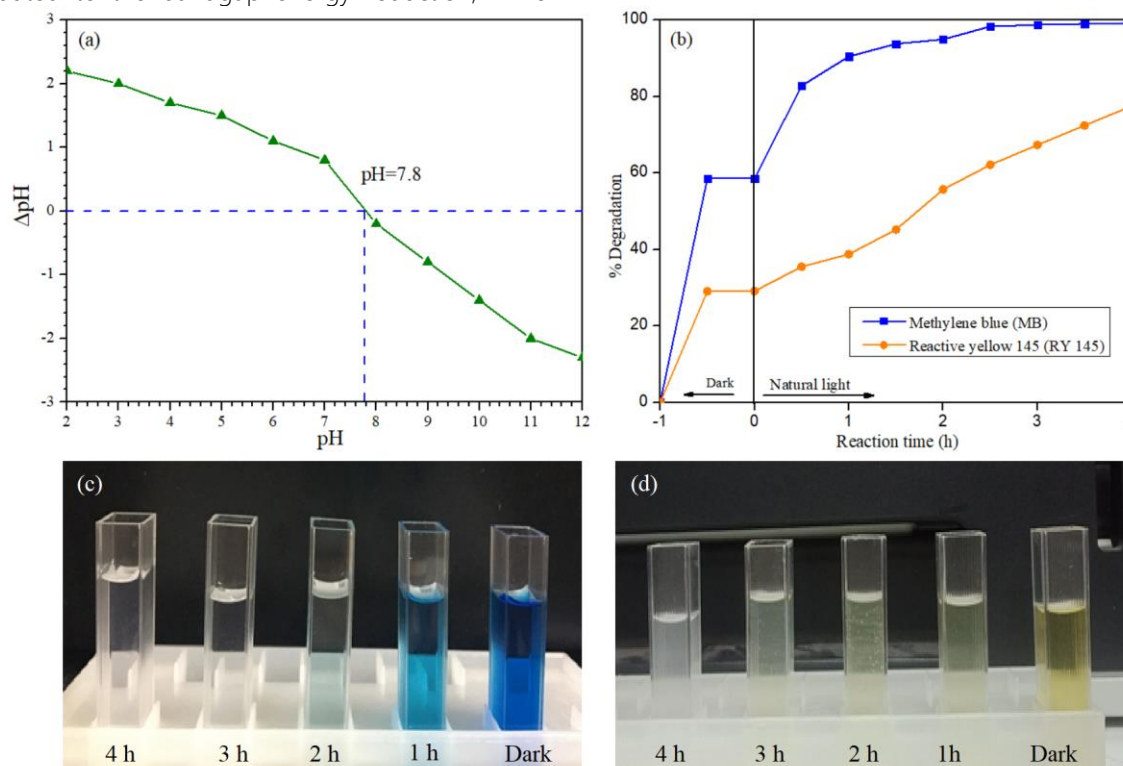


Figure 6: (a) Point of zero charge of 0.1Ag-Ag<sub>3</sub>PO<sub>4</sub>/Cellulose aerogel, (b-d) The photocatalytic efficiency of 0.1Ag-Ag<sub>3</sub>PO<sub>4</sub>/Cellulose aerogel degradation of MB and RY 145 dyes

The pH value of point zero charge (pH<sub>pzc</sub>) was measured on 0.1Ag-Ag<sub>3</sub>PO<sub>4</sub>/Cellulose aerogel composite in various pH environments to survey the surface area. When the solids are dispersed in water with pH lower than pH<sub>pzc</sub>, the surface of the material has positive charge and negative charge when pH higher than pH<sub>pzc</sub>. In Fig.5a, the plot between ΔpH and initial pH value determined the point zero charge at pH = 7.8. The results showed Fig.5b that the 0.1Ag-Ag<sub>3</sub>PO<sub>4</sub>/Cellulose aerogel has good photodegradation for MB cationic dyes. Photodegradation reached 93.8 % after 1.5 h and reached 99 % after 3 h, while the degradation efficiency of anionic RY 145 dyes only reached 77 % after 4 h of irradiation with visible light. This may be due to the surface of aerogel material containing OH<sup>-</sup> groups facilitating the binding of cation dyes. Hence, the dye ions binding to the

adsorbent mainly involved electrostatic interaction between cationic dyes and negatively charged OH<sup>-</sup> groups. The mechanism of the adsorption process is physical adsorption depending on electrostatic interaction. Creating an interaction force with MB cation molecules [34] so the adsorbability of MB dye is better than anionic dye RY 145. The increasing interaction between pollutant and catalyst active sites led to increased photodegradation efficiency. Photodegradation of MB dye was selected to investigate the factors affecting the photocatalytic process of Ag-Ag<sub>3</sub>PO<sub>4</sub>/Cellulose aerogel materials.

Factors such as the contents of the active phase, dye concentration, H<sub>2</sub>O<sub>2</sub> dosage and catalyst stability were also investigated to evaluate the photocatalytic efficiency of the composite materials. The results are shown in Figure 7.

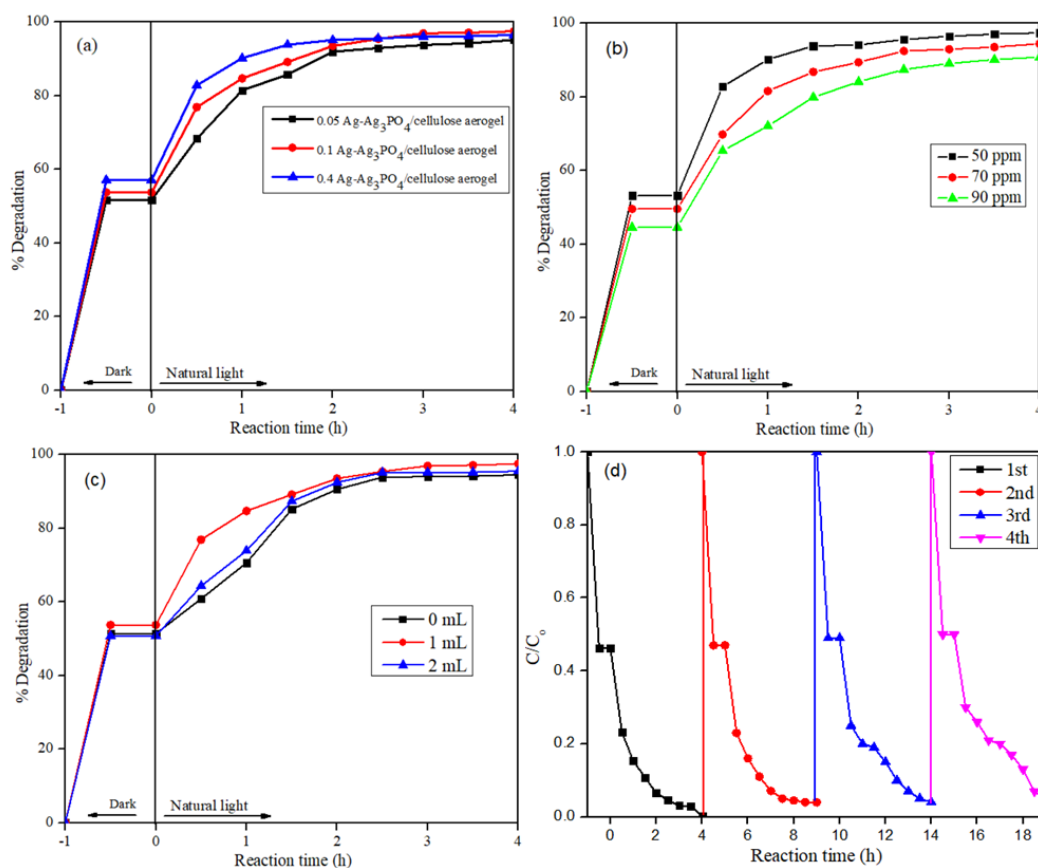


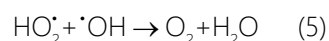
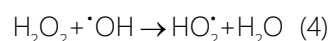
Figure 7: The degradation of MB dye under visible light using 0.1Ag-Ag<sub>3</sub>PO<sub>4</sub>/Cellulose aerogel catalyst under the conditions of (a) contents of the active phase, (b) dye concentration, (c) oxidant dosage (H<sub>2</sub>O<sub>2</sub>), (d) photocatalyst regenerability

The effect of Ag-Ag<sub>3</sub>PO<sub>4</sub>/Cellulose aerogel ratio on MB dye degradation efficiency is shown in Figure 7a. Photocatalytic efficiency was approximately 97% after 4 h, corresponding to 0.1Ag-Ag<sub>3</sub>PO<sub>4</sub>/Cellulose aerogel catalyst. With 0.4Ag-Ag<sub>3</sub>PO<sub>4</sub>/Cellulose aerogel catalyst, the efficiency after 4 h reached 96.5 %. With a large amount of AgNO<sub>3</sub>, the formation of active sites increased, but the interaction between the surface layers of the material occurred, thus reduced the formation of photo-produced electron-hole pairs of inside layers, led to a reduced photocatalytic efficiency.

To evaluate the effect of dye concentration on the photodegradation efficiency of Ag-Ag<sub>3</sub>PO<sub>4</sub>/Cellulose aerogel, the experiment was conducted with MB concentrations in the range of 50 to 90 ppm. The effect of initial concentration on the adsorption efficiency is shown in Figure 7b. The results showed that when the concentration of MB increased from 50 ppm to 90 ppm, the adsorption efficiency in the absence of light of 0.1Ag-Ag<sub>3</sub>PO<sub>4</sub>/Cellulose aerogel decreased from 53 % to 44 %. This can be due to the adsorbability of cellulose aerogel is inversely proportional to the dye concentration. After 4 h of

illumination with visible light, the 50 ppm dye sample had a treatment efficiency of 97 %, decreased to 94 % and 90 % for 70 ppm and 90 ppm samples, respectively.

The dosage of oxidizing agent H<sub>2</sub>O<sub>2</sub> also plays a large role in the degradation of MB dye by 0.1Ag-Ag<sub>3</sub>PO<sub>4</sub>/Cellulose aerogel composite (Figure 7c). The MB dye degradation efficiency increased with increasing oxidizing agent dosage: from 92 % in the absence of an oxidizing agent to 97% when using 1 mL of H<sub>2</sub>O<sub>2</sub>. However, when the H<sub>2</sub>O<sub>2</sub> content increased to 1.5 mL, the degradation efficiency decreased to 95 % after 4 h of illumination. This may be due to the presence of many free radicals  $\cdot\text{OH}$  created from H<sub>2</sub>O<sub>2</sub> promoted the reaction and led to faster degradation and higher efficiency. However, increasing the dosage of H<sub>2</sub>O<sub>2</sub> too much will result in the reduction of free radicals, according to the equation:



Additionally, a high dosage of H<sub>2</sub>O<sub>2</sub> also saturated the active sites of the catalyst, which decreased the reaction rate.

The regenerability of a photocatalyst is vital for its practical application. To evaluate these properties of 0.1Ag-Ag<sub>3</sub>PO<sub>4</sub>/Cellulose aerogel composite, the degradation of MB dye using 0.1Ag-Ag<sub>3</sub>PO<sub>4</sub>/Cellulose aerogel catalyst was repeated 4 times (Figure 7d). The degradation efficiency of MB dye only decreased slightly (reached 95%) after 4 consecutive runs. This has demonstrated the stability of this catalyst in the photodegradation process.

From the survey results of affecting factors: reaction temperature 30 °C, 50 mg of the catalyst, pH = 6.5 were used to investigate the kinetics of MB

photodegradation. The assumption that the reaction is first-order was established based on the equation:

$$-\ln\left(\frac{C_t}{C_0}\right) = k_p t \quad (6)$$

In which C<sub>t</sub> and C<sub>0</sub> are the concentration of the dye at time t and initial time (t=0), k<sub>p</sub> is the first-order rate constant. Figure 8 shows that the linearity of the plot ln(C<sub>0</sub>/C<sub>t</sub>) compared to the irradiation time (t), proved that the first-order reaction is consistent with the photodegradation reaction. Specifically, the value of the regression coefficient R<sup>2</sup> > 0.98. The reaction rate constant decreased from 1.2893 min<sup>-1</sup> to 0.6978 min<sup>-1</sup> when the dye concentration increased from 50 ppm to 90 ppm.

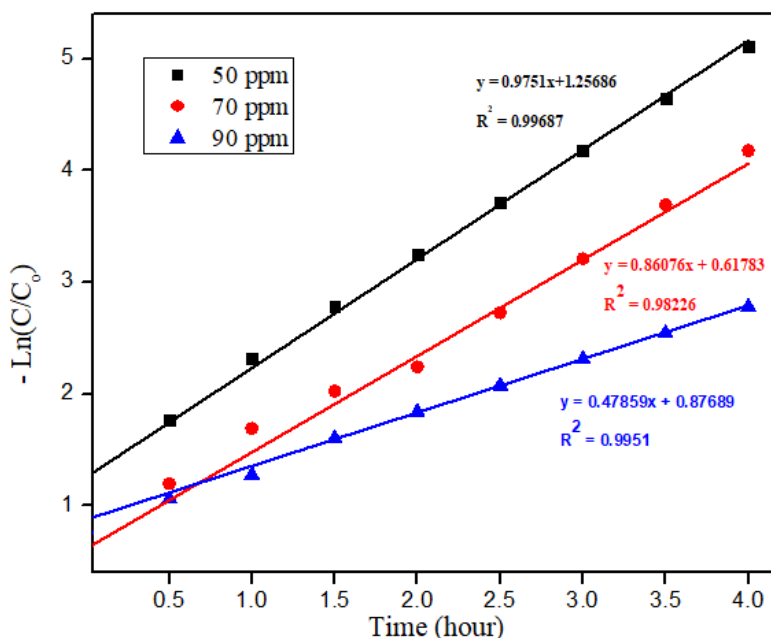
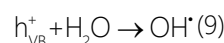
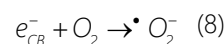


Figure 8: First-order kinetics model for 0.1Ag-Ag<sub>3</sub>PO<sub>4</sub>/Cellulose aerogel sample

The dye degradation mechanism of Ag-Ag<sub>3</sub>PO<sub>4</sub>/Cellulose aerogel composite could be similar to previous reports [35,36]. Ag and Ag<sub>3</sub>PO<sub>4</sub> nanoparticles absorb visible light effectively. Silver nanoparticles have two main roles in photocatalytic reactions: (i) enhance the charge transfer and prevent the recombination of photogenerated electron – hole pairs and (ii) increase the efficiency of photodegradation due to electrons produce from the surface plasmon effect. Furthermore, a large quantity of electron - hole pairs generated inside Ag<sub>3</sub>PO<sub>4</sub>, electrons in the valance band will jump onto the conduction band of Ag<sub>3</sub>PO<sub>4</sub> first and then to Ag particles. The remaining electrons trapped by O<sub>2</sub>

molecules on the catalyst surface will create <sup>•</sup>O<sub>2</sub><sup>-</sup> and holes react with H<sub>2</sub>O or OH<sup>-</sup> to create OH<sup>•</sup>. Those are the primary oxidants to degrade dye molecules into intermediate compounds along with CO<sub>2</sub> and H<sub>2</sub>O.



## Conclusions

In this study, Ag-Ag<sub>3</sub>PO<sub>4</sub>/Cellulose aerogel composite was synthesized successfully by hydrothermal reduction and freeze-drying method. The composite catalyst was studied systematically by MB and RY 145 degradation under visible light. Combining Ag<sub>3</sub>PO<sub>4</sub> nanoparticles and cellulose resulted in the decrease of the bandgap energy, thus prevented the recombination of the photogenerated electron-hole pairs and greatly improved the photocatalytic efficiency. The photocatalyst is highly stable, the degradation efficiency of MB remained at 99% after 4 consecutive runs, and the photocatalytic process of Ag-Ag<sub>3</sub>PO<sub>4</sub>/Cellulose aerogel material consisted of the first-order reaction model. Using bagasse to synthesis cellulose will help to reduce environmental pollution and make agricultural waste economically valuable.

## Acknowledgments

This work was supported by the National Foundation for Science and Technology Development of Vietnam (Nafosted) No. 105.99-2018.301. Hoa Thi Nguyen was funded by Vingroup Joint Stock Company by the Domestic Master/PhD Scholarship Programme of Vingroup Innovation Foundation (VINIF), Vingroup Big Data Institute (VINBIGDATA), code VINIF. 2020. ThS. 19.

## References

1. J. G. Mahy, L. Tasseroul, A. Zubiaur, J. Geens, M. Brisbois, M. Herlitschke, R. Herman, B. Heinrichs, and S. D. Lambert, Highly dispersed iron xerogel catalysts for p-nitrophenol degradation by photo-Fenton effects, *Microporous Mesoporous Mater.*, 197 (2014) 164-173. <https://doi.org/10.1016/j.micromeso.2014.06.009>
2. X. Guan, S. Lin, J. Lan, J. Shang, W. Li, Y. Zhan, H. Xiao, and Q. Song, Fabrication of Ag/AgCl/ZIF-8/TiO<sub>2</sub> decorated cotton fabric as a highly efficient photocatalyst for degradation of organic dyes under visible light, *Cellulose*, 26 (2019), 7437–7450. <http://dx.doi.org/10.1007/s10570-019-02621-8>
3. X. Chen, S. Shen, L. Guo, and S. S. Mao, Semiconductor-based photocatalytic hydrogen generation," *Chem. Rev.*, 110 (2010) 6503-6570. <https://doi.org/10.1021/cr1001645>
4. J. A. Byrne, P. S. M. Dunlop, J. W. J. Hamilton, P. Fernández-Ibáñez, I. Polo-López, P. K. Sharma and A. S. M. Vennard, A review of heterogeneous photocatalysis for water and surface disinfection, *Molecules*, 20 (2015) 5574-5615. <https://doi.org/10.3390/molecules20045574>
5. X. Fu, J. Wang, D. Huang, S. Meng, Z. Zhang, L. Li, T. Miao, and S. Chen, Trace Amount of SnO<sub>2</sub>-Decorated ZnSn(OH)<sub>6</sub> as Highly Efficient Photocatalyst for Decomposition of Gaseous Benzene: Synthesis, Photocatalytic Activity, and the Unrevealed Synergistic Effect between ZnSn(OH)<sub>6</sub> and SnO<sub>2</sub>, *ACS Catal.*, 6 (2016) 957-968. <https://doi.org/10.1021/acscatal.5b02593>
6. P. Zhang, X. Yang, Z. Zhao, B. Li, J. Gui, D. Liu, and J. Qiu, One-step synthesis of flowerlike C/Fe<sub>2</sub>O<sub>3</sub> nanosheet assembly with superior adsorption capacity and visible light photocatalytic performance for dye removal, *Carbon N. Y.*, 116 (2017) 59-67. <https://doi.org/10.1016/j.carbon.2017.01.087>
7. X. Yu, L. Gao, J. Huang, W. Li, G. Liu, Z. Li, J. Liu, and P. Hu, Construction of hybrid Ag<sub>2</sub>CO<sub>3</sub>/AgVO<sub>3</sub> nanowires with enhanced visible light photocatalytic activity, *Mater. Res. Bull.*, 101 (2018) 246-252. <https://doi.org/10.1016/j.materresbull.2018.01.023>
8. B. Luo, M. Chen, Z. Zhang, J. Xu, D. Li, D. Xu, and W. Shi, Highly efficient visible-light-driven photocatalytic degradation of tetracycline by a Z-scheme gC<sub>3</sub>N<sub>4</sub>/Bi<sub>3</sub>TaO<sub>7</sub> nanocomposite photocatalyst," *Dalt. Trans.*, 46 (2017) 8431-8438. <http://dx.doi.org/10.1039/C7DT01250K>
9. Z. Yi, J. Ye, N. Kikugawa, T. Kako, S. Ouyang, H. Stuart-Williams, H. Yang, J. Cao, W. Luo, Z. Li, Y. Liu and R. L. Withers, An orthophosphate semiconductor with photooxidation properties under visible-light irradiation, *Nat. Mater.*, 9 (2010) 559-564. <https://doi.org/10.1038/nmat2780>
10. J. Wang, F. Teng, M. Chen, J. Xu, Y. Song, and X. Zhou, Facile synthesis of novel Ag<sub>3</sub>PO<sub>4</sub> tetrapods and the {110} facets-dominated photocatalytic activity, *CrystEngComm*, 15 (2013) 39-42. <https://doi.org/10.1039/C2CE26060C>
11. M. A. Gondal, X. Chang, E. I. Wei, Z. H. Yamani, and Q. Zhou, Enhanced photoactivity on Ag/Ag<sub>3</sub>PO<sub>4</sub> composites by plasmonic effect, *J. Colloid Interface Sci.*, 392 (2013) 325–330. <https://doi.org/10.1016/j.jcis.2012.09.086>
12. Y. Liu, L. Fang, H. Lu, Y. Li, C. Hu, and H. Yu, One-pot pyridine-assisted synthesis of visible-light-driven photocatalyst Ag/Ag<sub>3</sub>PO<sub>4</sub>," *Appl. Catal. B Environ.*, 115 (2012) 245–252. <https://doi.org/10.1016/j.apcatb.2011.12.038>
13. X. Q. Liu, W. J. Chen, and H. Jiang, Facile synthesis of Ag/Ag<sub>3</sub>PO<sub>4</sub>/AMB composite with improved photocatalytic performance," *Chem. Eng. J.*, 308 <https://doi.org/10.51316/jca.2021.062>

- (2017) 889-896.  
<https://doi.org/10.1016/j.ccej.2016.09.125>
14. B. Liu, Z. Li, S. Xu, T. Cong, L. Tian, C. Ding, and M. Lu, "in situ synthesis of Ag@ Ag<sub>3</sub>PO<sub>4</sub>/MWCNT triples hetero-photocatalyst for degradation of malachite green," *Mater. Lett.*, 131 (2014) 229–232. <https://doi.org/10.1016/j.matlet.2014.05.214>
  15. L. Xu, W. Q. Huang, L. L. Wang, G. F. Huang, and P. Peng, Mechanism of superior visible-light photocatalytic activity and stability of hybrid Ag<sub>3</sub>PO<sub>4</sub>/graphene nanocomposite," *J. Phys. Chem. C*, 118 (2014) 12972–12979. <http://dx.doi.org/10.1021/jp5034273>
  16. G. Li and L. Mao, Magnetically separable Fe<sub>3</sub>O<sub>4</sub>-Ag<sub>3</sub>PO<sub>4</sub> sub-micrometre composite: Facile synthesis, high visible light-driven photocatalytic efficiency, and good recyclability," *RSC Adv.*, 2 (2012) 5108-5111. <https://doi.org/10.1039/c2ra20504a>
  17. L. Zhang, H. Zhang, H. Huang, Y. Liu, and Z. Kang, Ag<sub>3</sub>PO<sub>4</sub>/SnO<sub>2</sub> semiconductor nanocomposites with enhanced photocatalytic activity and stability," *New J. Chem.*, 36 (2012) 1541–1544. <https://doi.org/10.1039/C2NJ40206H>
  18. H. Yu, Z. Jiao, H. Hu, G. Lu, J. Ye, and Y. Bi, Fabrication of Ag<sub>3</sub>PO<sub>4</sub>-PAN composite nanofibers for photocatalytic applications," *CrystEngComm*, 15 (2013) 4802-4805. <https://doi.org/10.1039/c3ce00073g>
  19. N. Tavker, U. K. Gaur, and M. Sharma, Agro-waste extracted cellulose supported silver phosphate nanostructures as a green photocatalyst for improved photodegradation of RhB dye and industrial fertilizer effluents, *Nanoscale Adv.*, (2020). <https://doi.org/10.1039/d0na00181c>
  20. F. Chen, S. Li, Q. Chen, X. Zheng, P. Liu, and S. Fang, 3D graphene aerogels-supported Ag and Ag@Ag<sub>3</sub>PO<sub>4</sub> heterostructure for the efficient adsorption-photocatalysis capture of different dye pollutants in water, *Mater. Res. Bull.*, 105 (2018) 334-341. <https://doi.org/10.1016/j.materresbull.2018.05.013>
  21. S. Dong, L. Cui, C. Liu, F. Zhang, K. Li, L. Xia, X. Su, J. Feng, Y. Zhu, and J. Sun, Fabrication of 3D ultra-light graphene aerogel/Bi<sub>2</sub>WO<sub>6</sub> composite with excellent photocatalytic performance: A promising photocatalysts for water purification, *J. Taiwan Inst. Chem. Eng.*, 97 (2019) 288–296.
  22. J. Cai, S. Kimura, M. Wada, S. Kuga, and L. Zhang, Cellulose aerogels from aqueous alkali hydroxide-urea solution, *ChemSusChem*, 1 (2008) 149-154. <https://doi.org/10.1002/cssc.200700039>
  23. W. Chen, H. Yu, Q. Li, Y. Liu, and J. Li, Ultralight and highly flexible aerogels with long cellulose nanofibers, *Soft Matter*, 7 (2011) 20360-20368. <https://doi.org/10.1039/c1sm06179h>
  24. G. Tang, Z. G. Jiang, X. Li, H. Bin Zhang, A. Dasari, and Z. Z. Yu, Three dimensional graphene aerogels and their electrically conductive composites, *Carbon N. Y.*, 77 (2014) 592-599. <https://doi.org/10.1016/j.carbon.2014.05.063>
  25. Q. B. Thai, S. T. Nguyen, D. K. Ho, T. D. Tran, D. M. Huynh, N. H.N. Do, T. P. Luu, P. K. Le, D. K. Le, N. P. Thien, H. M. Duong, Cellulose-based aerogels from sugarcane bagasse for oil spill-cleaning and heat insulation applications," *Carbohydr. Polym.*, 228 (2020). <https://doi.org/10.1016/j.carbpol.2019.115365>
  26. A. L. Patterson, The scherrer formula for X-ray particle size determination, *Phys. Rev.*, 56 (1939) 978-982. <https://doi.org/10.1103/PhysRev.56.978>
  27. A. Kumar, B. Prasad, and I. M. Mishra, Adsorptive removal of acrylonitrile by commercial grade activated carbon: Kinetics, equilibrium and thermodynamics, *J. Hazard. Mater.*, 152 (2008) 589-600. <https://doi.org/10.1016/j.jhazmat.2007.07.048>
  28. M. C. Silva, O. R. Lopes, J. L. Colodette, A. O. Porto, J. Rieumont, D. Chaussy, M. N. Belgacemd, and G. G. Silva, Characterization of three non-product materials from a bleached eucalyptus kraft pulp mill, in view of valorising them as a source of cellulose fibres, *Ind. Crops Prod.*, 27 (2008) 288-295. <https://doi.org/10.1016/j.indcrop.2007.11.005>
  29. Y. Xu, H. Xu, J. Yan, H. Li, L. Huang, Q. Zhang, C. Huang, and H. Wan, A novel visible-light-response plasmonic photocatalyst CNT/Ag/AgBr and its photocatalytic properties, *Phys. Chem. Chem. Phys.*, 15 (2013) 5821-5830. <https://doi.org/10.1039/c3cp44104k>
  30. Y. Min, G. He, Q. Xu, and Y. Chen, Self-assembled encapsulation of graphene oxide/Ag@ AgCl as a Z-scheme photocatalytic system for pollutant removal, *J. Mater. Chem. A*, 2 (2014) 1294–1301. <https://doi.org/10.1039/C3TA13687F>
  31. J. Cai, S. Kimura, M. Wada, and S. Kuga, Nanoporous cellulose as metal nanoparticles support, *Biomacromolecules*, 10 (2009) 87-94. <https://doi.org/10.1021/bm800919e>
  32. S. Liu, D. Ke, J. Zeng, J. Zhou, T. Peng, and L. Zhang, Construction of inorganic nanoparticles by micro-nano-porous structure of cellulose matrix, *Cellulose*, 18 (2011) 945-956. <https://doi.org/10.1007/s10570-011-9556-5>
- <https://doi.org/10.51316/jca.2021.062>

33. P. Kubelka and F. Munk, Ein Beitrag zur Optik der Farbanstriche, *Zeitschrift für Tech. Phys.*, (1931). <https://doi.org/10.4236/msce.2014.28004>
34. L. X. Zhong, X. W. Peng, D. Yang, and R. C. Sun, Adsorption of heavy metals by a porous bioadsorbent from lignocellulosic biomass reconstructed in an ionic liquid, *J. Agric. Food Chem.*, 60 (2012) 5621-5628. <https://doi.org/10.1021/jf301182x>
35. W. Teng, X. Li, Q. Zhao, J. Zhao, and D. Zhang, In situ capture of active species and oxidation mechanism of RhB and MB dyes over sunlight-driven Ag/Ag<sub>3</sub>PO<sub>4</sub> plasmonic nanocatalyst, *Appl. Catal. B Environ.*, 125 (2012) 538–545. <https://doi.org/10.1016/j.apcatb.2012.05.043>
36. B. Jiang, Y. Wang, J. Q. Wang, C. Tian, W. Li, Q. Feng, Q. Pan, and H. Fu, InSitu Fabrication of Ag/Ag<sub>3</sub>PO<sub>4</sub>/Graphene Triple Heterostructure Visible-Light Photocatalyst through Graphene-Assisted Reduction Strategy, *ChemCatChem*, 5 (2013) 1359-1367. <https://doi.org/10.1002/cctc.201200684>